Retinal MMP-12, MMP-13, TIMP-1, and TIMP-2 Expression in Murine Experimental Retinal Detachment

Bongsu Kim,[1] Mohamed H. Abdel-Rahman,[1–3] Tiffany Wang,[1] Severin Pouly,[1] Ashraf M. Mahmoud,[1] and Colleen M. Cebulla[1]

[1]Havener Eye Institute, Department of Ophthalmology and Visual Science, The Ohio State University, Columbus, Ohio, United States
[2]Division of Human Genetics, The Ohio State University, Columbus, Ohio, United States
[3]Department of Pathology, Menoufiya University, Shebin Elkom, Egypt

Correspondence: Colleen M. Cebulla, Havener Eye Institute, The Ohio State University, Department of Ophthalmology and Visual Science, 915 Olentangy River Road, Suite 5000, Columbus, OH 43212, USA; Colleen.Cebulla@osumc.edu.

BK and MHA-R contributed equally to the work presented here and should therefore be regarded as equivalent authors.

Submitted: October 1, 2013
Accepted: January 31, 2014

Citation: Kim B, Abdel-Rahman MH, Wang T, Pouly S, Mahmoud AM, Cebulla CM. Retinal MMP-12, MMP-13, TIMP-1, and TIMP-2 expression in murine experimental retinal detachment. *Invest Ophthalmol Vis Sci*. 2014;55:2031–2040. DOI:10.1167/iovs.13-13374

Purpose. Matrix metalloproteinases (MMPs) and their inhibitors play a role in the pathobiology of retinal detachment (RD) and proliferative vitreoretinopathy (PVR). Proliferative vitreoretinopathy is facilitated by chronic retinal detachment and involves excessive deposition of extracellular matrix (ECM) proteins. Matrix metalloproteinase-2 and -13 are important modulators of the ECM which have not been evaluated in RD. The purpose of this study was to investigate the retinal expression of select MMPs, including MMP-12, MMP-13, and associated inhibitors in a murine model of retinal detachment.

Methods. Transient or chronic retinal detachments (RDs) were induced by subretinal injection of either saline (SA) or hyaluronic acid (HA) in C57BL/6 mice. To confirm that the HA-RD model has features consistent with PVR-like changes, glial activation and subretinal fibrosis were evaluated with immunofluorescence, dilated fundus examination, and spectral-domain optical coherence tomography (SD-OCT). Gene expression was quantified by qRT-PCR. Proteins were assayed by immunoblot and immunohistochemistry.

Results. Hyaluronic acid RD eyes developed gliosis and subretinal fibrosis on dilated exam, SD-OCT, and immunofluorescence analysis. Gene expression of *Mmp-12* and *Mmp-13*, and *Timp-1* was strongly upregulated at all time points in RD compared with controls. *Timp-2*, *Mmp-2*, and *Mmp-9* expression was modest. Hyaluronic acid RDs exhibited more MMP and TIMP expression than SA-RDs. MMP-12, -13, and TIMP-1 proteins were elevated in RDs compared with controls. Immunohistochemistry revealed moderate to strong MMP-13 levels in subretinal space macrophages.

Conclusions. Fibrosis can develop in the HA-RD model. There is an upregulation of select MMPs that may modulate the wound healing process following RD.

Keywords: retinal detachment, proliferative vitreoretinopathy, extracellular matrix, matrix metalloproteinase, tissue inhibitor metalloproteinase, MMP-13, MMP-12, TIMP-1, TIMP-2, spectral-domain optical coherence tomography

Retinal detachments (RDs) are an important clinical cause of visual loss, with an annual incidence of 12.4 per 100,000.[1] The visual consequences of RD are particularly dismal in those 5% to 10% who develop proliferative vitreoretinopathy (PVR).[2] Proliferative vitreoretinopathy formation is more likely in RDs with long duration,[3] vitreous hemorrhage, large or giant retinal tears, multiple retinal breaks, choroidal detachment, previous failed attempts at reattachment, signs of uveitis, and penetrating trauma.[2,4,5] It involves cellular proliferation and migration of retinal pigment epithelial cells and Müller glia, accumulation of inflammatory infiltrate and fibroblast-like cells, excessive deposition of extracellular matrix (ECM) proteins, and an interaction of these cells with the ECM.[4,6–10] The wound healing response in RD is thought to include a balance of matrix deposition and removal, with activity of matrix metalloproteinases (MMPs) and their inhibitors.

The MMPs and tissue inhibitors of metalloproteinases (TIMPs) are key modulators of the extracellular matrix (ECM). The MMPs are a family of enzymes that degrade specific ECM components and include stromelysins (MMP-3 and -10); collagenases (MMP-1 [interstitial collagenase], -8 [neutrophil collagenase], and -13 [collagenase 3]); gelatinases (MMP-2 and -9); transmembrane MMPs (MT-MMPs: MMP-14, -15, -16, and -24); and macrophage metalloelastase (MMP-12).[11,12] Since there is increased ECM deposition and contraction in PVR, there is considerable interest in the local MMP and TIMP expression in RDs.

Macrophages are an important source of MMPs, and some of the most interesting, yet less-understood, include MMP-12 and MMP-13.[13,14] MMP-12 was first identified in alveolar macrophages from smokers[15] and was recently identified in a proteomic analysis of individuals with PVR.[16] Matrix metalloproteinase-13, particularly from scar-associated macrophages, appears to be important in fibrosis resolution in a liver injury model.[14] In the eye, MMP-13 produced by bone marrow–derived cells appears important in choroidal neovascular

membrane formation, which can lead to scar formation.[17] The modulation of fibrosis by MMP-12 and -13 in a wide variety of models is interesting since it could have implications for the development of PVR.[14,18–20] Since the accumulation of macrophages is a prominent feature in RD, we hypothesized that MMP-12 and -13 are produced during RD. To our knowledge, MMP-12 and MMP-13 expression have not been evaluated in retinal detachment.

The purpose of this study was to investigate the retinal gene expression of MMP-12 and MMP-13 relative to other select MMPs and TIMPs in animal models of both transient and chronic RDs, the latter of which facilitate the conditions for PVR development; and to determine the expression kinetics and localization of retinal MMP-12, MMP-13, and associated inhibitors TIMP-1 and TIMP-2 in a murine model of retinal detachment. Notably, the chronic murine RD model created by subretinal hyaluronic acid (HA) injection has already been shown in the literature to have features of PVR, including glial activation and subretinal gliosis.[21–23] We also show data, including with spectral domain optical coherence tomography (SD-OCT), that scarring can develop in this model.

Methods

Animals and Retinal Detachment Surgery

This research adheres to the principles of the ARVO Statement for the Use of Animals in Ophthalmic and Vision Research. It was conducted under a protocol approved by The Ohio State University Institutional Animal Care and Use Committee. Retinal detachments were induced by subretinal injection of approximately 5 μL undiluted HA (10 mg/mL; Abbott Medical Optics, Santa Ana, CA, USA) or sterile saline (SA) into left eyes of 22- to 24-week-old C57BL/6 mice as previously described.[24] Mice were anesthetized with intraperitoneal injection of ketamine (90 mg/kg) and xylazine (10 mg/kg). Pupils were dilated with tropicamide 1%. Eyes were prepped with betadine and a 30-gauge (g) needle was used to make the entry site for a 33-g, 19-mm custom Hamilton needle (Hamilton Company, Reno, NV, USA), approximately 2 mm posterior to the limbus in the superotemporal quadrant. Anterior chamber tap with a 30-g needle was performed to reduce the intraocular pressure and then the subretinal HA or SA injection was performed with the aid of an operating microscope to create a total or near-total RD. Eyes were treated with erythromycin ophthalmic ointment. Untreated right eyes served as controls.

Fundus Evaluation and SD-OCT Imaging

Retinas ($n = 40$ HA-RD mice) were viewed with an operating microscope through a dilated pupil to determine presence or absence of subretinal fibrosis (whitish subretinal plaques or linear structures) prior to tissue harvest. In a subset of 2-week-old, HA-RD mice with clinical evidence from dilated fundus examination of subretinal fibrosis ($n = 6$), right and left eyes were imaged with SD-OCT (Bioptigen, Durham, NC, USA) as previously described[24] to document subretinal fibrosis prior to tissue harvest.

Enucleation, Fixation, and Retina Isolation

Anesthetized mice were euthanized and eyes enucleated. Retinas were dissected using 0.12 forceps and Vannas scissors to cut the anterior cap of the eye. The retina was gently separated from the underlying RPE and choroid, and was cut near the insertion into the optic nerve. Retinas were processed for RNA and protein isolation.

For immunohistochemistry, the eyes were enucleated and a small opening was cut in the temporal limbus to allow better penetration of fixative. The eye was placed in fixative containing phosphate buffer with 4% paraformaldehyde and 3% sucrose in 0.1 M phosphate buffer at pH 7.4 for 30 minutes. Eyes were washed twice in PBS for 10 minutes and placed in 30% sucrose in PBS overnight. The eyes were embedded in optimal cutting temperature solution (Electron Microscopy Sciences, Hatfield, PA, USA), snap frozen, and cut into 12-μm sections.

Quantitative Real-Time (qRT)-PCR

For gene expression studies, the total RNA was extracted from retinas at each time point ($n = 4$–5 retinas pooled per group) using TRIZOL (Invitrogen, Carlsbad, CA, USA) per the manufacturer's instructions. Ribonucleic acid was quantitated and 260/280 ratio was determined using a plate reader (Epoch; BioTek, Winooski, VT, USA). The cDNA was synthesized using a commercial kit (SuperScript VILO cDNA Synthesis Kit; Invitrogen) with a thermal cycler (C-1000; Bio-Rad Laboratories, Inc., Hercules, CA, USA) according to the manufacturer's instructions. Gene expression of murine *Mmp12* (assay ID number Mm00500554_m1); *Mmp13* (Mm00439491_m1); *Mmp2* (Mm00439498_m1); *Mmp9* (Mm00442991_m1); *Timp1* (Mm00441818_m1); and *Timp2* (Mm00441825_m1) was quantified by qRT-PCR by using catalogued probes (Taqman; Applied Biosystems [ABI], Foster City, CA, USA) using 3-μg cDNA template in a 15-μL reaction volume. Samples were loaded in triplicate on 96-well plates and analyzed with a real-time PCR system (ABI Prism 7900HT Fast Real-Time PCR System; Applied Biosystems) at the Nucleic Acids Core facility at Ohio State. Threshold cycle (*Ct*) values were normalized to *Gapdh* (assay ID number NM_008084.2) and analyzed using the ΔΔCt method[25]; standard deviations were calculated.

Western Blot

Total protein was collected from individual isolated retinas (control and HA-RD from each mouse) at weeks 1, 2, or 3 through 4. Retinas were homogenized with cold extraction buffer (120 mM Tris-HCl [pH 8.7], 0.1% Triton X-100, and 5% glycerol).[26] Proteins were quantitated using the Bradford method. Equal microgram quantities of protein were suspended in Laemmli buffer with β-mercaptoethanol and fractionated with SDS-PAGE on 4% to 20% precast gels (Invitrogen). Proteins were electroblotted onto a polyvinylidene fluoride membrane (Bio-Rad Laboratories, Inc.). Membranes were blocked with 5% milk and immunoblotted for MMP-12 (EP1261Y rabbit monoclonal IgG, carboxyterminal; Abcam, Cambridge, England); MMP-13 (VIIIA2 mouse monoclonal IgG1; Millipore Corp., Billerica, MA); TIMP-1 (H-150 rabbit polyclonal; Santa Cruz Biotechnology, Inc., Dallas, TX, USA); and TIMP-2 (anti-C-terminus rabbit polyclonal catalogue #AB2965; Millipore Corp.). Blots were developed using ECL or SuperSignal (Pierce Biotechnology, Rockford, IL, USA) chemiluminescence. Blots were stripped and α-tubulin expression was evaluated as a loading control to normalize the data. Films were scanned with a flatbed scanner (Epson Stylus NX400; Epson, Suwa, Nagano Prefecture, Japan) at 600 dpi and Java-based imaging software (ImageJ; National Institutes of Health, Bethesda, MD, USA) was used to determine band densitometry. Ratios of protein of interest to loading control protein areas were determined for the individual RD and fellow-eye retinal pairs for the week 1, week 2, and weeks 3 through 4 time points, respectively: $n = 10$, 10, and 9 pairs for MMP-13; $n = 10$, 10, and 9 for MMP-12; $n = 7$, 6, and 6 for

TIMP-1; and $n = 7$, 7, and 7 for TIMP-2. Standard deviations of the adjusted ratios were determined.

Immunohistochemistry (IHC)

Immunofluorescence was performed as previously described in HA-RD eyes.[27] Reactive glia and subretinal scars were detected with anti-glial fibrillary acidic protein (GFAP, clone IB4; AbD Serotec, Oxford, UK). Slides were blocked with PBS containing 5% bovine serum albumin, and 1% Triton-X 100. AlexaFluor 488 or 568 conjugated secondary antibodies were used (1:1000; Invitrogen) after 30 minutes of incubation with 100% normal goat serum. Omission of the primary antibody was used as a control for background staining; omission of primary and secondary antibodies was used as a control for autofluorescence. Cell nuclei were counterstained with 4′,6-diamidino-2-phenylindole (DAPI).

Immunoperoxidase IHC was performed to detect MMPs, TIMPs, and macrophages since autofluorescence was a confounding factor in the subretinal space for these markers. Goat IgG 1 μg/mL (Vector Laboratories, Burlingame, CA, USA) in blocking solution was applied to block Fc receptors. Antibodies listed above were used to detect MMP-12, MMP-13, TIMP-1, TIMP-2, and F4/80 (rat monoclonal, IgG2b; AbD Serotec) was used to detect macrophages. Secondary goat anti-rat, -rabbit (Invitrogen), or -mouse (minimal x-reactivity; BioLegend, San Diego, CA, USA) conjugated with horseradish peroxidase were applied. A commercial enzyme substrate kit (ImmPACT NovaRED; Vector Laboratories) was used to visualize the markers. Hematoxylin was used as a counterstain. HeLa cells grown on coverslips were used as a positive control for MMP-12 immunostaining.

Image Analysis

Photomicrographs were obtained using a fluorescent microscope (Leica DM5000B; Leica Microsystems, Wetzlar, Germany) and digital camera (Leica DC500; Leica Microsystems) or a clinical microscope (Nikon Eclipse 50i; Nikon Corp., Tokyo, Japan) and a microscope camera controller (Nikon Digital Sight DS-U1; Nikon Corp.) with commercial software (NIS-Elements; Nikon Corp.) for immunoperoxidase images. Images were optimized for color, brightness, and contrast. For immunoperoxidase labeling, adjacent slides were evaluated for expression of MMP-12, F4/80, MMP-13, and TIMP-1. Sections from at least four different animals at the area of detachment were evaluated. To minimize the variability of region-specific differences within the retina, the same region of the retina was evaluated for the fellow eye control and retinal detachment areas. Identical illumination, microscope, and camera settings were used. Fixed areas were randomly sampled across all retinal layers in areas of detachment or similar control retina areas. The retina was selected as the region of interest from the ×200 field of view. Subretinal fibrosis was measured using a modification of Lewis et al.[28] Continuous cellular growth located sclerad to the outer limiting membrane that were GFAP positive with DAPI-positive nuclei were measured (height, length, and number) per mm^2 of retina with a graphics editing program (Adobe Photoshop 6.0; Adobe Systems, San Jose, CA, USA). Immunofluorescence of retinal GFAP was quantified using image analysis software (Image-Pro 6.2; Media Cybernetics, Inc., Rockville, MD, USA) as previously described.[29] Identical illumination, microscope, and camera settings were used to obtain images for quantification. Fixed areas were sampled from 5.4-megapixel digital images. These areas were randomly sampled across all retinal layers in areas of detachment or similar control retina areas. The total area of retinal GFAP immunofluorescence was calculated for regions with pixel intensities above a determined threshold and averaged per group. The average density was calculated as the mean pixel value above threshold within threshold-designated regions.

Statistical Analysis

Averages of GFAP relative density and subretinal scar measurements were determined. Error bars represent SEM and significance was determined with paired *t*-test with $P < 0.05$ considered significant. To determine whether differences in Western blot proteins were significant, ANOVA was first performed to confirm a difference in measurements with $P < 0.05$ considered significant. Subsequent post hoc analysis with paired *t*-test was performed ($P \leq 0.017$ was considered significant using Bonferroni correction). Fold changes in normalized protein levels were determined from paired control and RD samples and averaged. Statistical software (SAS version 9.2; SAS Institute, Inc., Cary, NC, USA) was used for analyses.

Results

Gliosis and Subretinal Fibrosis in Murine HA-RD

There are several reports that suggest the chronic HA-RD murine model develops some features of PVR, including activation of the Müller glia and extension of glial processes below the external limiting membrane.[21–23] To confirm that our model of chronic HA-RD develops some features consistent with PVR, the presence of retinal fibrosis was evaluated clinically, as well as with immunofluorescence, and SD-OCT. Dilated fundus examination with the operating microscope in 40 mice with 2- or 4-week HA-RDs ($n = 28$ and 12, respectively) was performed prior to tissue harvest. Five 2-week-old eyes were excluded due to mature cataract. Areas clinically consistent with subretinal fibrosis were seen in the majority of all RD eyes (26/35, 74.3% overall: 60.9% of 2-week-old and 100% of 4-week-old eyes), while 4/35 (11.4%) had no identifiable fibrosis. In 5/35 (14.3%) the presence or absence of fibrosis could not be determined because of cataract or preretinal hemorrhage. Pre-retinal fibrosis was not identified clinically in these eyes.

Microscopically, the relative GFAP density was increased in detached areas at 2 and 4 weeks ($n = 4$ per group), compared with matched-control retinas, reaching statistical significance in 2-week-old RDs ($P = 0.0346$; Fig. 1). Similar to other reports, glial processes extending beneath the external limiting membrane were identified in some detached areas (Fig. 1E). Subretinal scars were identified in both 2- and 4-week RD samples ($n = 4$ per group) and were absent in control retinas (Fig. 1).

A subset of mice thought to have clinical evidence of subretinal scar ($n = 6$) were evaluated with SD-OCT (Figs. 1K–O). Two mice did not have adequate images to interpret. Of mice with good quality images, three out of four had areas consistent with subretinal fibrosis indicated by hyper-reflective thickened areas sclerad to the outer nuclear layer and anterior to the retinal pigment epithelium (Fig. 1). Two mice had evidence of "finger-like" intraretinal fibrotic projections (Figs. 1M, 1N) and areas of preretinal fibrosis. The mouse without clear subretinal fibrosis had a large RD with undulation of the outer retina. In one detached region, focally increased hyper-reflectivity and tighter undulation was suspicious for speculative subretinal gliosis (Fig. 1O).

MMP and TIMP Gene Expression in Transient and Chronic Murine RDs

Saline RDs are transient, lasting approximately 24 hours,[22] while HA-RDs are chronic.[24,30] To evaluate gene expression in these

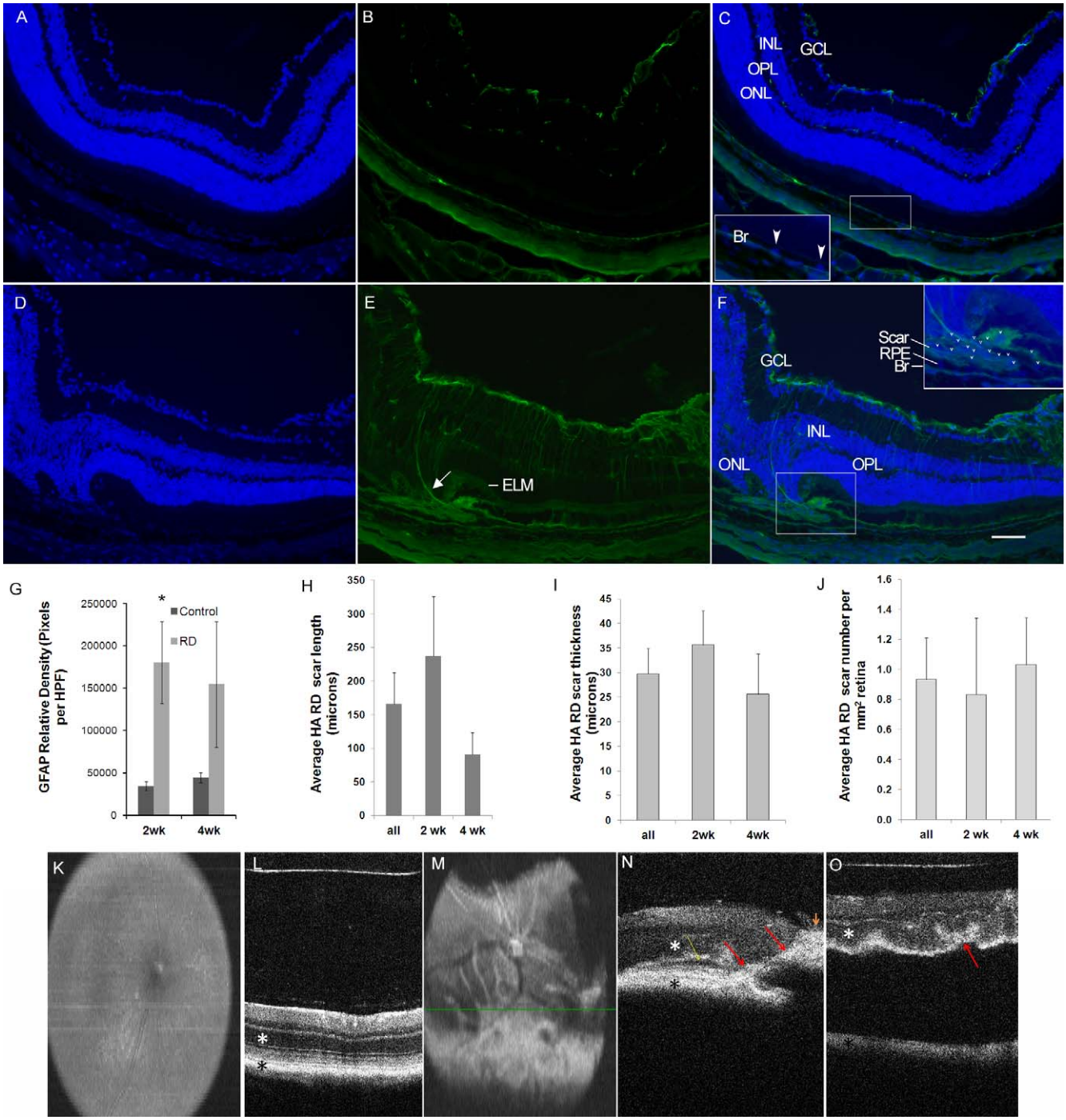

Figure 1. Gliosis and fibrosis in the murine HA-RD model. Glial fibrillary acidic protein immunofluorescence (*green*, [**B**, **C**, **E**, **F**]) with increased GFAP expression in RD retinas (**E**, **F**) compared with the untreated fellow eye (**B**, **C**). DAPI is used as a nuclear counterstain (*blue*, [**A**, **C**, **D**, **F**]). The inset in (**C**) shows the DAPI-positive RPE in the control eye (*blue*, *arrowheads*). There is extension of a glial process (*arrow*, [**E**]) below the external limiting membrane (ELM), which is somewhat difficult to visualize in the area overlying the subretinal scar. The inset in (**F**) shows a subretinal scar in 2-week RD positive for GFAP and containing DAPI positive nuclei (many labeled with *arrowheads*). Glial fibrillary acidic protein is elevated in RD retinas at 2 and 4 weeks ([**G**], *asterisk*: $P < 0.05$). Subretinal fibrosis was outlined and average scar length, thickness, and number of scars was quantitated for all, 2-week, and 4-week RDs (**H**–**J**). Spectral-domain OCT B-scan images are labeled with a *white asterisk* marking the outer nuclear layer and a *black asterisk* marking the RPE band. Spectral-domain OCT en face (**K**) and B-scan (**L**) images of a control eye show normal nerve, vessels, and retinal architecture. The fellow HA-RD eye shows subretinal fibrosis inferior to the optic nerve in the en face image (**M**) with whitish linear and placoid structures; the B-scan image (**N**) is located superior to the indicator line from the en face image in (**M**). *Red arrows* mark the white subretinal and intraretinal fibrosis; *yellow arrow* marks the small subretinal fluid (dark layer below the white photoreceptor layer); and *orange arrowhead* marks the white preretinal fibrosis with shadowing posteriorly (**N**). Another HA-RD eye shows prominent RD with undulation of the outer retina and focal shortening in an area of undulations ([**O**], *red arrow*). Br, Bruch's membrane; GCL, ganglion cell layer; INL, inner nuclear layer; ONL, outer nuclear layer; OPL, outer plexiform layer.

Table. Fold Change Compared With Control of All Retinal Gene Expression in Both SA- and HA-RDs

Gene	Control Fold Change ± SD	SA-RD Fold Change ± SD	HA-RD Fold Change ± SD
Mmp-2			
1 d	1 ± 0.2	2.1 ± 0.2	2.1 ± 0.2
1 wk	1 ± 0.1	0.8 ± 0.2	1.5 ± 0.1
2 wk	1 ± 0.1	2.4 ± 0.1	2.7 ± 0.5
5 wk	1 ± 0.3	ND	1.5 ± 0.5
Mmp-9			
1 d	1 ± 0.2	1.1 ± 0.1	1.3 ± 0.1
1 wk	1 ± 0.1	1.3 ± 0.1	1.6 ± 0.2
2 wk	1 ± 0.2	1.1 ± 0.1	2.4 ± 0.5
5 wk	1 ± 0.2	ND	1.2 ± 0.5
Mmp-12			
1 d	1 ± 0.1	76.6 ± 0.3	86.5 ± 0.1
1 wk	1 ± 0.2	0.3 ± 0.1	8.6 ± 0.1
2 wk	1 ± 0.6	13.9 ± 0.1	57.1 ± 0.5
5 wk	1 ± 0.2	ND	13.3 ± 0.5
Mmp-13			
1 d	1 ± 0.1	13.4 ± 0.1	9.3 ± 0.1
1 wk	1 ± 0.2	0.4 ± 0.4	2.2 ± 0.1
2 wk	1 ± 0.2	12.3 ± 0.2	208.3 ± 0.5
5 wk	1 ± 0.2	ND	10.7 ± 0.5
Timp-1			
1 d	1 ± 0.1	1.7 ± 0.2	1.5 ± 0.1
1 wk	1 ± 0.3	0.9 ± 0.3	2.0 ± 0.2
2 wk	1 ± 0.2	2.9 ± 0.1	85.4 ± 0.5
5 wk	1 ± 0.3	ND	4.3 ± 0.5
Timp-2			
1 d	1 ± 0.2	1.9 ± 0.2	1.4 ± 0.1
1 wk	1 ± 0.2	0.8 ± 0.2	1.2 ± 0.2
2 wk	1 ± 0.1	1.0 ± 0.1	2.7 ± 0.5
5 wk	1 ± 0.2	ND	1.4 ± 0.6

ND, not done.

different conditions, *Mmp* and *Timp* gene expression was evaluated in short-term and chronic RDs at day 1 and weeks 1 and 2. Hyaluronic acid RDs were also evaluated at week 5. Gene expression of *Mmp-12*, *Mmp-13*, and *Timp-1* was strongly upregulated in RD eyes compared with controls, while *Mmp-2*, *Mmp-9*, and *Timp-2* were modestly upregulated (Table, Fig. 2). Matrix metalloproteinase and TIMP gene expression was greater in HA-RDs compared with SA-RDs. *Mmp-12* had the earliest upregulation, with maximal expression at day 1 in both SA- and HA-RD eyes. Expression was sustained at 2 weeks and was 4-fold greater in HA-RDs than SA-RDs. In contrast, *Mmp-13* expression peaked later than *Mmp-12*; it was increased maximally at 2 weeks with 17-fold greater expression in HA compared with SA-RDs (Fig. 2). Similarly, *Timp-1* was maximally elevated at week 2 and was 29 times higher in HA-RDs than SA-RDs (Fig. 2). There were smaller maximal increases in gene expression in SA- and HA-RD eyes compared with controls for *Mmp-2*, *Mmp-9*, and *Timp-2. Mmp-2* expression remained elevated at 2 weeks in both SA- and HA-RDs at equivalent levels, while *Mmp-9* expression decreased slightly in SA-RDs compared with HA-RDs at 2 weeks. Sustained gene expression was detected in HA-RDs at 5 weeks in *Mmp-12*, *Mmp-13*, *Timp-1*, and *Mmp-2*, while gene expression of *Mmp-9* and *Timp-2* returned to near baseline levels (Fig. 2). Similar results were found in an independent replicate (not shown).

MMP and TIMP Western Blot in HA-RD

To determine whether MMP-12, MMP-13, and TIMPs were upregulated at the protein level as well as the level of gene expression, Western blot analysis was performed on 1-, 2-, and 3- to 4-week HA-RDs and controls (Fig. 3). Western analysis showed similar results to the gene expression studies: MMP-12 and MMP-13 levels were higher in RD eyes compared with controls. Matrix metalloproteinase-12 increased the earliest, with a 245% increase above paired controls at 1 week ($P = 0.0345$, borderline significant, Fig. 3), while differences at the other time points were not significant. Matrix metalloproteinase-12 levels in the RDs subsequently declined, with greater protein levels at 1 week compared with 3 weeks ($P = 0.0886$, borderline significant). Matrix metalloproteinase-13 expression was more sustained, with highest expression at the 1-week time point compared with controls (427% increase above paired controls at 1 week, $P = 0.0023$; 194% increase at 2 weeks, $P = 0.1061$; and 181% increase at 3 weeks, $P = 0.0059$, Fig. 3). Levels of MMP-13 were not significantly different between the RD groups at the three different time points ($P = 0.52$).

Western blot revealed increased expression of TIMP-1, but not TIMP-2, in RDs compared with controls (Fig. 2). Tissue inhibitor of metalloproteinase-1 increased in 1- and 2-week RDs compared with paired controls (436% at week 1, $P = 0.0092$; 905% at week 2, $P = 0.0499$; and 266% at week 3, $P = 0.204$). Tissue inhibitor of metalloproteinase-2 levels were similar in control and RD eyes and did not increase significantly after RD.

MMP Immunohistochemistry in HA-RD

To further evaluate where MMP and TIMP expression occurred in RD eyes, immunohistochemistry was performed. Immunoperoxidase immunostaining revealed increased levels of MMP-13 in subretinal macrophages, as shown by F4/80 IHC (Fig. 4). Tissue inhibitor of metalloproteinase-1 and MMP-12 were not detected. A positive control for MMP-12 (HeLa cells) showed good reactivity of the human cells (not shown). Tissue inhibitor of metalloproteinase-2 was detected homogenously in the inner retina, primarily in the inner plexiform layer and outer plexiform layer equally in both control and RD eyes (not shown).

Discussion

To our knowledge, this is the first study to document subretinal fibrosis in the HA-RD murine model with SD-OCT and the first detailed analysis of MMP-12, MMP-13, and TIMP expression in this animal model of RD. Regarding the timing of gene expression in experimental RD, we found that *Mmp-12* and *Mmp-13* are both expressed in transient saline RDs, which last approximately 1 day, as well as in the chronic HA-RD, which is a prevalent model for studying retinal detachment[30,31] and facilitates the conditions for development of fibrosis in PVR. This model is well-studied regarding accumulation of macrophages into the retina and subretinal space, similar to human RD.[24,32–37] *Mmp-13* gene expression was greatest in the chronic HA-RDs at 2 weeks. The kinetics of maximal *Mmp-12* gene expression occurred earlier than those of *Mmp-13*, although expression of both genes was sustained. This significant and persistent gene expression of *Mmp-12* and *Mmp-13* is similar to results in a thioacetamide rat liver fibrosis model, in which *Mmp-12* and *Mmp-13* were expressed at high levels acutely, during the injury phase, with lower levels expressed during the model's fibrotic phase (55-fold expression decreased to approximately 10-fold and 80-fold to approximately 10-fold, respectively).[18]

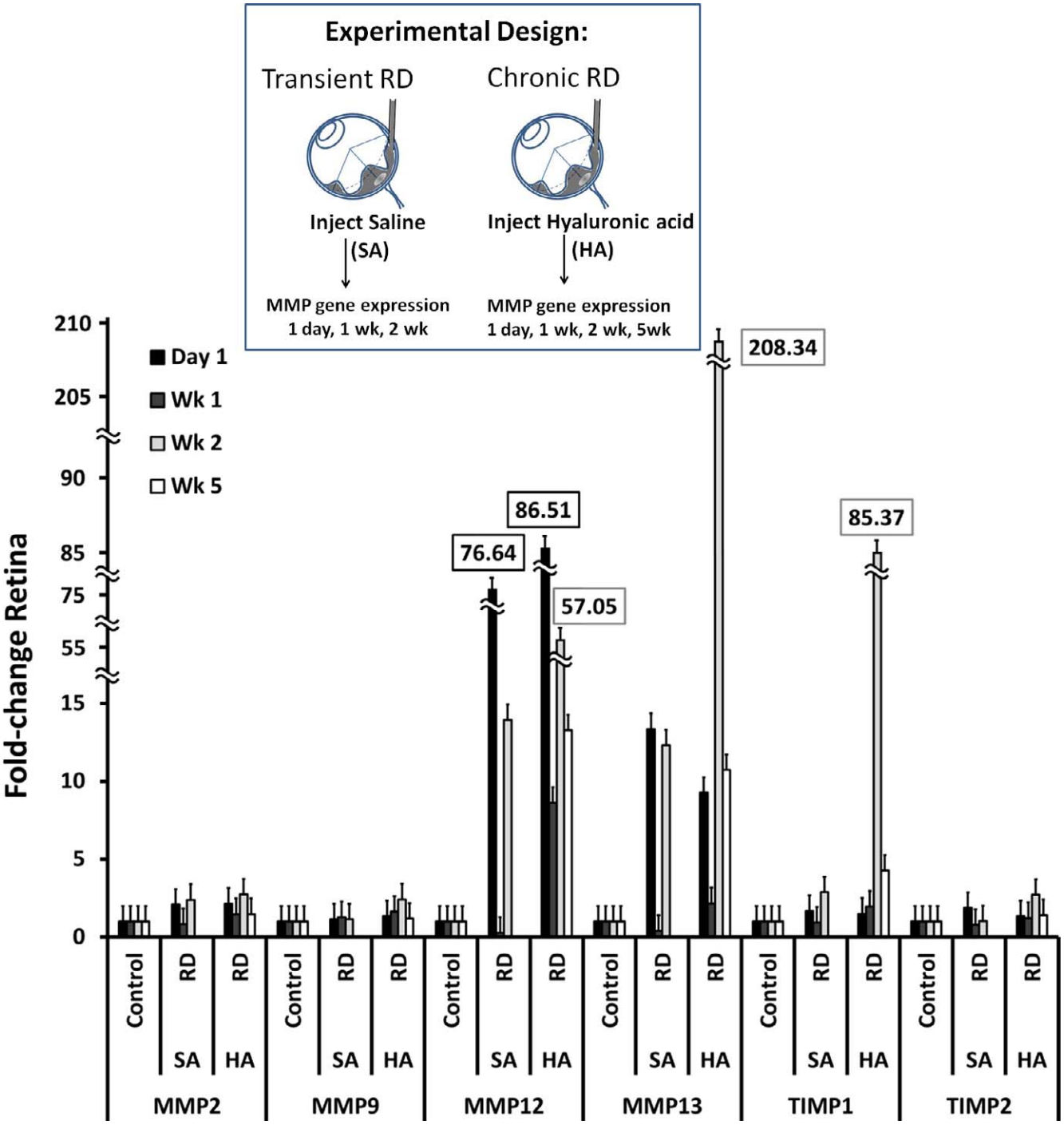

Figure 2. Increased gene expression of select MMPs and TIMPs in transient and chronic RDs. Gene expression by qRT-PCR in SA- and HA-RDs compared with control eyes at day 1, week 1, week 2, and week 5 (HA-RD only). Four to five retinas were pooled per group to evaluate gene expression in each experimental condition. *Error bars* represent standard deviation.

Interestingly, we detected much lower levels of *Mmp-2* and *Mmp-9* gene expression than *Mmp-12* and *-13* in the time points evaluated. This is surprising since MMP-2 and MMP-9 have been reported to be upregulated in human retinal detachment and PVR samples.[38–46] However, most of the studies that have evaluated MMP-2 and -9 in RD have evaluated them at the protein level. We hypothesize that the elevated protein levels of these MMPs may be due to post-transcriptional changes rather than increased gene expression. Alternately, we may have missed the time point of maximally elevated gene expression.

In our RD model, protein expression of MMP-12 and -13 mirrored gene expression, with some exceptions. There was a borderline-significant early upregulation of MMP-12 at 1 week, but no sustained increase on Western blot. There was a significant, more sustained upregulation of MMP-13 at all time points. The physiologic inhibitors of MMP-12 and -13 showed differential expression kinetics in RD. Importantly, TIMP-1 upregulation paralleled MMP-12 and -13 expression, with

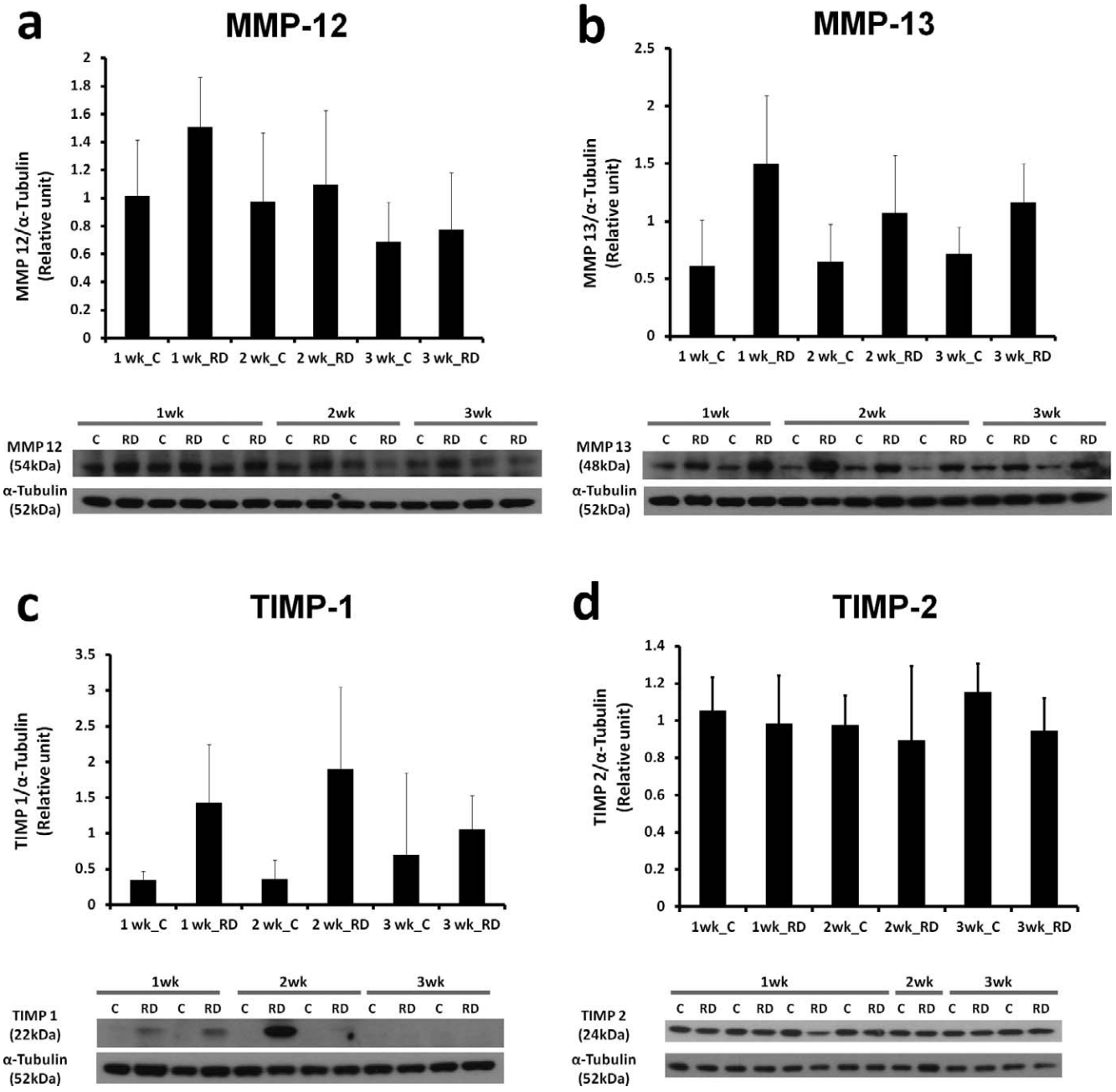

FIGURE 3. Time course of increased MMP-12, MMP-13, TIMP-1, and TIMP-2 proteins in HA-RD. Western blots and accompanying histograms of densitometry analysis show increases in MMP-12 (**a**), MMP-13 (**b**), TIMP-1 (**c**), and TIMP-2 (**d**). Densitometry analysis normalized values to alpha-tubulin and represents the average of individual retinas. (**a**) $n = 10$, 10, and 9 individual retinas for the 1-, 2-, and 3- to 4-week time points, respectively. (**b**) $n = 10$, 10, and 9 individual retinas for the 1-, 2-, and 3- to 4-week time points, respectively. (**c**) $n = 7$, 6, and 6 individual retinas per time point, respectively. (**d**) $n = 7$, 7, and 7 individual retinas per time point, respectively). *Error bars* represent standard deviation.

increases at the early and mid-time points. Conversely, moderate TIMP-2 levels, detected by a C-terminus antibody, were present at all time points with no difference between control and RD retinas. Thus, differential TIMP-1 expression may play a greater role in dynamic ECM remodeling in experimental RD. Similar findings of TIMP-1 gene expression kinetics were found in a murine skin wound-healing model, with no expression in normal skin and increased expression in early wound time points.[47] In contrast, TIMP-2 expression was constitutive and was not modulated during wound healing.[47] It is tempting to hypothesize that scar remodeling and regression could result from the sustained expression of MMP-13 as TIMP-1 declines at later time points.

We hypothesized that subretinal macrophages in detached retina would express MMP-12 and MMP-13. Consistent with this, MMP-13 localized to subretinal macrophages on immunohistochemical analysis. These results are similar to other studies showing that macrophages are an important source of MMP-13 after tissue injury.[14] Surprisingly, MMP-12 was not detected in subretinal macrophages, despite elevated MMP-12 levels on Western blot and q-PCR at early time points. Species differences may explain why MMP-12 was not detected on IHC in the murine retina but was detected in the human HeLa cells

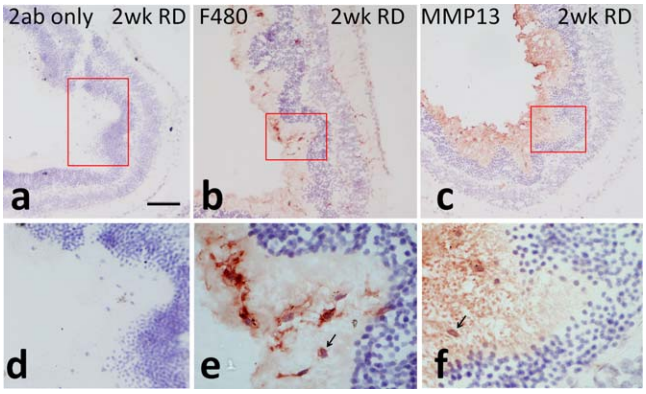

FIGURE 4. Immunoperoxidase localization of MMP-13 in experimental RD. Insets (**d**) through (**f**) show magnified images of the highlighted areas from (**a**) through (**c**), respectively. Secondary only controls show no significant background staining in 2-week HA-RDs ([**a**, **d**], ×100 and ×200 magnification, respectively). Macrophages and microglia were detected with F4/80, particularly in the subretinal space in detached areas as well as inner and outer plexiform layers ([**b**, **e**], ×100 and ×1000 magnification, respectively). There was expression of MMP-13 (*red* in [**c**, **f**], ×100 and ×1000 magnification, respectively) in subretinal macrophages (*arrow*) in detached areas. *Scale bar*: 50 μm.

used as a positive control. It is also possible that a greater elevation in MMP-12 protein levels occurred earlier and that our analysis took place as levels were declining. Paradoxically, MMP-12 was recently identified in the vitreous by a mass spectrometric analysis as a key node in an interaction network of PVR, which is a late complication of RD.[16] While confirmation with Western blot or ELISA is needed to validate those results, it suggests that MMP-12 expression could also be a late event associated with extensive proliferative membranes (e.g., vitreous from advanced PVR group C and D eyes was evaluated).

Because PVR, the most feared complication of RD, is a profibrotic wound healing response, the expression of MMPs and TIMPs is of major interest. In PVR, there is deposition and organization of numerous ECM components. With disruption of the blood retinal barrier, there is deposition of a temporary layer of serum-derived fibronectin and fibrin, which is replaced by collagen and cell-derived fibronectin with regulation by TGFβ.[48] Collagens, predominantly type I and III but also II, IV, and V, have been described in PVR membranes.[49] Fibronectin, laminin, vitronectin, tenascin, thrombospondin-1, osteonectin, and integrins have also been detected in PVR membranes.[48–50] Several studies have identified RPE, fibroblasts, and inflammatory cells, such as macrophages, and lymphocytes.[8,9,51] It is thought the ECM interacts with the cells in the matrix, especially the RPE, to promote migration of cells and later contraction of the fibrotic membranes.[49]

Matrix metalloproteinase-12 and MMP-13 are both capable of acting on many of the ECM components of PVR. For example, MMP-13 ECM substrates include types I, II, III, IV, IX, X, XIV collagen (preferential for type II), gelatin, large tenascin C, fibronectin, aggrecan, laminin, versican and fibrillin, and osteonectin.[11,12] Matrix metalloproteinase-12 substrates include elastin, gelatins, collagen IV, laminin, fibronectin, and protoglycan.[12] Interestingly, MMP-12 and −13 can activate other MMPs; MMP-12 can activate MMP-2 while MMP-13 can activate both MMP-2 and MMP-9.[11] This activation of other MMPs may contribute to the upregulation of MMP-2 and MMP-9 seen in clinical RDs.[38–44] Future work should be done to test this hypothesis.

It is unclear whether selective MMP inhibitors could be beneficial or detrimental in RDs with high risk for PVR. Evaluations of MMP-13 reveal both pro- and antifibrotic activity, depending on timing and disease model evaluated. Several studies suggest MMP-13 expression reduces fibrosis. In a carbon tetrachloride (CCL_4) model of mouse liver fibrosis, an MMP-13 expression plasmid with a hyaluronic acid coating decreased liver fibrosis.[19] In another CCL_4 model, MMP-13$^{-/-}$ mice had slower regression of fibrosis in the recovery phase, although regression of fibrosis was not blocked completely.[14] Importantly, scar-associated macrophages were identified as a major source of MMP-13 associated with fibrosis resolution in this model.

In contrast to the CCL_4 model, MMP-13 deficiency was found to have an antifibrotic effect in a different murine liver fibrosis model (bile duct ligation [BDL] cholestasis model).[20] BDL was followed by analysis at day 5 (acute) and week 3 (chronic) time points. Acutely, MMP13$^{-/-}$ mice had reduction in inflammation, TIMP-1 and profibrotic gene expression, and MMP-2 and -9 activities. Importantly, in the chronic phase, MMP13$^{-/-}$ mice had decreased hepatic fibrosis and collagen content, and decreased hepatic stellate cell proliferation and myofibroblastic phenotype. The authors suggest that the timing of MMP-13 activity in liver fibrosis models is critical to whether it promotes or inhibits fibrosis; the studies that have found a benefit of MMP-13 in reducing liver fibrosis with collagenase-expressing adenoviral vectors delivered during the spontaneous recovery phase when the fibrosis-inducing agent was removed. In contrast, expression of MMP-13 during the initial injury phase is associated with inflammation and increased liver fibrosis. Thus, the timing of MMP-13 activity may be harmful early, by causing liver inflammation, despite a beneficial effect on fibrosis in the recovery phase.

Proliferative vitreoretinopathy results from a complex cascade of events. Strategies to prevent and treat PVR will require a multimodal, combinatorial approach. It is unknown what role MMPs and TIMPs play in this process. It is likely that specific MMPs and their inhibitors have different effects depending on the timing of expression and ratios with inhibitors. Future studies of MMP-12 and MMP-13 in human RD surgical vitreous and subretinal fluid specimens and studies with knockout mice will be important to determine the potential impact of these important MMPs in RD.

Acknowledgments

The authors thank Andy J. Fischer for his comments. We thank Bioptigen for providing a demonstration of the small animal imaging SD-OCT.

Supported by the National Eye Institute of the National Institutes of Health under Award Number K08EY022672 and by Award Number KL2TR001068 from the National Center For Advancing Translational Sciences. The content is solely the responsibility of the authors and does not necessarily represent the official views of these institutions. Additional funds were provided by the Ohio Lions Eye Research Foundation, Fund #313310 in Ophthalmology, and the Patti Blow Fund.

Disclosure: **B. Kim**, None; **M.H. Abdel-Rahman**, None; **T. Wang**, None; **S. Pouly**, None; **A.M. Mahmoud**, None; **C.M. Cebulla**, Bioptigen (F)

References

1. Haimann MH, Burton TC, Brown CK. Epidemiology of retinal detachment. *Arch Ophthalmol*. 1982;100:289–292.
2. Asaria RH, Charteris DG. Proliferative vitreoretinopathy: developments in pathogenesis and treatment. *Compr Ophthalmol Update*. 2006;7:179–185.

3. Tseng W, Cortez RT, Ramirez G, Stinnett S, Jaffe GJ. Prevalence and risk factors for proliferative vitreoretinopathy in eyes with rhegmatogenous retinal detachment but no previous vitreoretinal surgery. *Am J Ophthalmol*. 2004;137:1105–1115.
4. Pastor JC, de la Rua ER, Martin F. Proliferative vitreoretinopathy: risk factors and pathobiology. *Prog Retin Eye Res*. 2002; 21:127–144.
5. Jalali S. Retinal detachment. *Community Eye Health*. 2003;16: 25–26.
6. Vinores SA, Campochiaro PA, Conway BP. Ultrastructural and electron-immunocytochemical characterization of cells in epiretinal membranes. *Invest Ophthalmol Vis Sci*. 1990;31: 14–28.
7. Charteris DG, Downie J, Aylward GW, Sethi C, Luthert P. Intraretinal and periretinal pathology in anterior proliferative vitreoretinopathy. *Graefes Arch Clin Exp Ophthalmol*. 2007; 245:93–100.
8. Charteris DG, Hiscott P, Grierson I, Lightman SL. Proliferative vitreoretinopathy. Lymphocytes in epiretinal membranes. *Ophthalmology*. 1992;99:1364–1367.
9. Charteris DG, Hiscott P, Robey HL, Gregor ZJ, Lightman SL, Grierson I. Inflammatory cells in proliferative vitreoretinopathy subretinal membranes. *Ophthalmology*. 1993;100:43–46.
10. Sethi CS, Lewis GP, Fisher SK, et al. Glial remodeling and neural plasticity in human retinal detachment with proliferative vitreoretinopathy. *Invest Ophthalmol Vis Sci*. 2005;46: 329–342.
11. Ala-aho R, Kahari VM. Collagenases in cancer. *Biochimie*. 2005;87:273–286.
12. Benyon RC, Arthur MJ. Extracellular matrix degradation and the role of hepatic stellate cells. *Semin Liver Dis*. 2001;21: 373–384.
13. Newby AC. Metalloproteinase expression in monocytes and macrophages and its relationship to atherosclerotic plaque instability. *Arterioscler Thromb Vasc Biol*. 2008;28:2108–2114.
14. Fallowfield JA, Mizuno M, Kendall TJ, et al. Scar-associated macrophages are a major source of hepatic matrix metalloproteinase-13 and facilitate the resolution of murine hepatic fibrosis. *J Immunol*. 2007;178:5288–5295.
15. Shapiro SD, Kobayashi DK, Ley TJ. Cloning and characterization of a unique elastolytic metalloproteinase produced by human alveolar macrophages. *J Biol Chem*. 1993;268:23824–23829.
16. Yu J, Peng R, Chen H, Cui C, Ba J. Elucidation of the pathogenic mechanism of rhegmatogenous retinal detachment with proliferative vitreoretinopathy by proteomic analysis. *Invest Ophthalmol Vis Sci*. 2012;53:8146–8153.
17. Lecomte J, Louis K, Detry B, et al. Bone marrow-derived mesenchymal cells and MMP13 contribute to experimental choroidal neovascularization. *Cell Mol Life Sci*. 2011;68:677–686.
18. Qin L, Han YP. Epigenetic repression of matrix metalloproteinases in myofibroblastic hepatic stellate cells through histone deacetylases 4: implication in tissue fibrosis. *Am J Pathol*. 2010;177:1915–1928.
19. Kim EJ, Cho HJ, Park D, et al. Antifibrotic effect of MMP13-encoding plasmid DNA delivered using polyethylenimine shielded with hyaluronic acid. *Mol Ther*. 2011;19:355–361.
20. Uchinami H, Seki E, Brenner DA, D'Armiento J. Loss of MMP 13 attenuates murine hepatic injury and fibrosis during cholestasis. *Hepatology*. 2006;44:420–429.
21. Nakazawa T, Takeda M, Lewis GP, et al. Attenuated glial reactions and photoreceptor degeneration after retinal detachment in mice deficient in glial fibrillary acidic protein and vimentin. *Invest Ophthalmol Vis Sci*. 2007;48:2760–2768.
22. Luna G, Kjellstrom S, Verardo MR, et al. The effects of transient retinal detachment on cavity size and glial and neural remodeling in a mouse model of X-linked retinoschisis. *Invest Ophthalmol Vis Sci*. 2009;50:3977–3984.
23. Verardo MR, Lewis GP, Takeda M, et al. Abnormal reactivity of Muller cells after retinal detachment in mice deficient in GFAP and vimentin. *Invest Ophthalmol Vis Sci*. 2008;49:3659–3665.
24. Cebulla CM, Ruggeri M, Murray TG, Feuer WJ, Hernandez E. Spectral domain optical coherence tomography in a murine retinal detachment model. *Exp Eye Res*. 2010;90:521–527.
25. Abdel-Rahman MH, Craig EL, Davidorf FH, Eng C. Expression of vascular endothelial growth factor in uveal melanoma is independent of 6p21-region copy number. *Clin Cancer Res*. 2005;11:73–78.
26. Ispanovic E, Serio D, Haas TL. Cdc42 and RhoA have opposing roles in regulating membrane type 1-matrix metalloproteinase localization and matrix metalloproteinase-2 activation. *Am J Physiol Cell Physiol*. 2008;295:C600–C610.
27. Cebulla CM, Jockovich ME, Pina Y, et al. Basic fibroblast growth factor impact on retinoblastoma progression and survival. *Invest Ophthalmol Vis Sci*. 2008;49:5215–5221.
28. Lewis GP, Chapin EA, Byun J, Luna G, Sherris D, Fisher SK. Muller cell reactivity and photoreceptor cell death are reduced after experimental retinal detachment using an inhibitor of the Akt/mTOR pathway. *Invest Ophthalmol Vis Sci*. 2009;50: 4429–4435.
29. Cebulla CM, Zelinka CP, Scott MA, et al. A chick model of retinal detachment: cone rich and novel. *PLoS One*. 2012;7: e44257.
30. Fisher SK, Lewis GP, Linberg KA, Verardo MR. Cellular remodeling in mammalian retina: results from studies of experimental retinal detachment. *Prog Retin Eye Res*. 2005; 24:395–431.
31. Fisher SK, Lewis GP. Muller cell and neuronal remodeling in retinal detachment and reattachment and their potential consequences for visual recovery: a review and reconsideration of recent data. *Vision Res*. 2003;43:887–897.
32. Nakazawa T, Hisatomi T, Nakazawa C, et al. Monocyte chemoattractant protein 1 mediates retinal detachment-induced photoreceptor apoptosis. *Proc Natl Acad Sci U S A*. 2007;104:2425–2430.
33. Hisatomi T, Sakamoto T, Sonoda KH, et al. Clearance of apoptotic photoreceptors: elimination of apoptotic debris into the subretinal space and macrophage-mediated phagocytosis via phosphatidylserine receptor and integrin alphavbeta3. *Am J Pathol*. 2003;162:1869–1879.
34. Kaneko H, Nishiguchi KM, Nakamura M, Kachi S, Terasaki H. Characteristics of bone marrow-derived microglia in the normal and injured retina. *Invest Ophthalmol Vis Sci*. 2008; 49:4162–4168.
35. Lewis GP, Sethi CS, Carter KM, Charteris DG, Fisher SK. Microglial cell activation following retinal detachment: a comparison between species. *Mol Vis*. 2005;11:491–500.
36. Lewis GP, Charteris DG, Sethi CS, Fisher SK. Animal models of retinal detachment and reattachment: identifying cellular events that may affect visual recovery. *Eye*. 2002;16:375–387.
37. Anderson DH, Stern WH, Fisher SK, Erickson PA, Borgula GA. Retinal detachment in the cat: the pigment epithelial-photoreceptor interface. *Invest Ophthalmol Vis Sci*. 1983; 24:906–926.
38. Kon CH, Occleston NL, Charteris D, Daniels J, Aylward GW, Khaw PT. A prospective study of matrix metalloproteinases in proliferative vitreoretinopathy. *Invest Ophthalmol Vis Sci*. 1998;39:1524–1529.
39. Gonzalez-Avila G, Mendez D, Lozano D, Ramos C, Delgado J, Iturria C. Role of retinal detachment subretinal fluid on extracellular matrix metabolism. *Ophthalmologica*. 2004;218: 49–56.
40. Symeonidis C, Papakonstantinou E, Androudi S, et al. Interleukin-6 and the matrix metalloproteinase response in the vitreous during proliferative vitreoretinopathy. *Cytokine*. 2011;54:212–217.
41. Symeonidis C, Papakonstantinou E, Souliou E, Karakiulakis G, Dimitrakos SA, Diza E. Correlation of matrix metalloproteinase

Investigative Ophthalmology & Visual Science

levels with the grade of proliferative vitreoretinopathy in the subretinal fluid and vitreous during rhegmatogenous retinal detachment. *Acta Ophthalmol*. 2011;89:339–345.

42. Symeonidis C, Diza E, Papakonstantinou E, Souliou E, Dimitrakos SA, Karakiulakis G. Correlation of the extent and duration of rhegmatogenous retinal detachment with the expression of matrix metalloproteinases in the vitreous. *Retina*. 2007;27:1279–1285.
43. Symeonidis C, Diza E, Papakonstantinou E, Souliou E, Karakiulakis G, Dimitrakos SA. Expression of matrix metalloproteinases in the subretinal fluid correlates with the extent of rhegmatogenous retinal detachment. *Graefes Arch Clin Exp Ophthalmol*. 2007;245:560–568.
44. Coral K, Angayarkanni N, Madhavan J, et al. Lysyl oxidase activity in the ocular tissues and the role of LOX in proliferative diabetic retinopathy and rhegmatogenous retinal detachment. *Invest Ophthalmol Vis Sci*. 2008;49:4746–4752.
45. De La Paz MA, Itoh Y, Toth CA, Nagase H. Matrix metalloproteinases and their inhibitors in human vitreous. *Invest Ophthalmol Vis Sci*. 1998;39:1256–1260.
46. Webster L, Chignell AH, Limb GA. Predominance of MMP-1 and MMP-2 in epiretinal and subretinal membranes of proliferative vitreoretinopathy. *Exp Eye Res*. 1999;68:91–98.
47. Madlener M. Differential expression of matrix metalloproteinases and their physiological inhibitors in acute murine skin wounds. *Arch Dermatol Res*. 1998;(suppl 290):S24–S29.
48. Pastor JC. Proliferative vitreoretinopathy: an overview. *Surv Ophthalmol*. 1998;43:3–18.
49. Hiscott P, Sheridan C, Magee RM, Grierson I. Matrix and the retinal pigment epithelium in proliferative retinal disease. *Prog Retin Eye Res*. 1999;18:167–190.
50. Hiscott P, Hagan S, Heathcote L, et al. Pathobiology of epiretinal and subretinal membranes: possible roles for the matricellular proteins thrombospondin 1 and osteonectin (SPARC). *Eye (Lond)*. 2002;16:393–403.
51. Tang S, Scheiffarth OF, Wildner G, Thurau SR, Lund OE. Lymphocytes, macrophages and HLA-DR expression in vitreal and epiretinal membranes of proliferative vitreoretinopathy. An immunohistochemical study. *Ger J Ophthalmol*. 1992;1:176–179.

Investigative Ophthalmology & Visual Science